WEMPEC

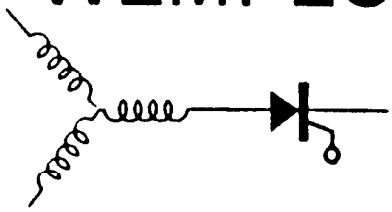

Wisconsin Electric Machines and Power Electronics Consortium

RESEARCH REPORT
85-7

A Modified Control Method For Fast Response Current Source Inverter Drives

D. Deng and T.A. Lipo
University of Wisconsin
1415 Johnson Drive
Madison, Wisconsin 53705

Department of Electrical and Computer Engineering
University of Wisconsin-Madison
Madison, Wisconsin 53706

A MODIFIED CONTROL METHOD FOR FAST RESPONSE CURRENT SOURCE INVERTER DRIVES

D. DENG and T. A. LIPO
University of Wisconsin
1415 Johnson Drive
Madison, Wisconsin 53706

ABSTRACT

The factors which influence the current response to a current command for a normal auto-sequentially commutated current link inverter (ASCI) are discussed. A simple new method of notching the output current waveform for the ASCI is presented, which is used to control the ac output current from the ASCI. To demonstrate the improvement in the current response of the ASCI with notching (or NASCI) two typical classes of control systems of ac induction machine drives are considered. A performance comparison is made between ASCI and NASCI induction machine drives. Analysis and analog computer simulation results show that substantial improvement in dynamic response is achieved when the notching is utilized.

INTRODUCTION

Inverters which function as a current source rather than a voltage source are rapidly becoming the dominant power structure for high performance ac motor drives. At lower power levels such a current source is obtained from a conventional pulse width modulated (PWM) voltage link inverter by tight closed loop control of the output currents. Because of the chopping mode of the inverter and the high gain of the overall current loop, the ac motor current can follow the current command signal very quickly. At higher power levels an auto-sequentially commutated current link inverter (ASCI) is typically employed. An important advantage of the ASCI is its inherent regenerating ability by use of dc link reactor and phase controlled bridge at the front end. However, in this case the response of the current loop is not the same as for the current regulated PWM voltage inverter. Control of the phase of the current, being derived from switching of the ASCI continues to be relatively rapid. The amplitude of the ac output current from inverter is now obtained by adjusting the magnitude of the dc link current. Because of the fairly large inductor in the dc link section, the current response to an input command is influenced very much by the dc link parameters. While response can be minimized by high gain in the rectifier current regulator loop, excessive gain can cause control problms due to saturation (limiting) of the rectifier output voltage as well as ripple current instabilities at light load. Hence, the current response of a conventional ASCI is substantially slower than for a current regulated PWM voltage inverter.

This paper investigates a new method to control the ac output current from the normal ASCI inverter which makes the current response of this converter structure much faster than the original response. In this scheme the dc link current remains fixed. Regulation of ac current amplitude is obtained by systematically bypassing the inverter output current by gating thyristors in both the top and bottom legs of a given phase. The power circuit remains the same as for the conventional ASCI inverter. The complexity of the control circuit for this new scheme also is not substantially different than for the normal ASCI. Hence, the benefits of the ASCI are again retained. Because the dc current is kept constant, the influence of the dc link parameters on the dynamics of the system response is negligible. Hence, rapid control of both ac current amplitude and phase can be obtained. The control response becomes essentially independent of both dc link and stator circuit parameters in much the same manner as the current regulated PWM voltage inverter.

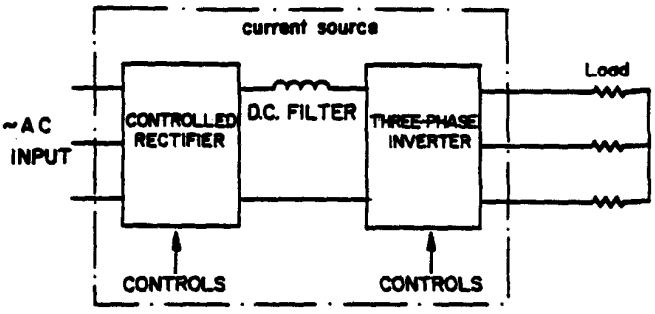

Fig. 1 Block Diagram of Basic Auto-Sequentially Commutated Current Source.

NOTCHING CONTROL METHOD

Figure 1 shows the block diagram of a basic current source system which includes a controlled rectifier, a dc current filter, and an auto-sequentially commutated current source inverter. Fig. 2 gives the power circuit of the inverter. The current source proposed in this paper includes the same components and power circuit as in Figs. 1 and 2. However, in this case the dc link current is assumed to be fixed and a special firing sequence of the inverter thyristors is used to provide a variable output current to the load. For convenience, it is useful to designate the operation of an ASCI under such control as a notched auto-sequentially commutated inverter, or simply as a NASCI inverter.

In order to explain the principle of operation of the NASCI it is sufficient to compare the firing method of this inverter to that of the standard ASCI. For clarity, the switching time of thyristors is ignored. Fig. 3 shows the time sequence of firing signals in the ASCI while Fig. 4 shows the output line current from the ASCI to the load. Each thyristor conducts for $2\pi/3$ radians during each half cycle. The resulting current from the ASCI is a square wave of current with width of $2\pi/3$ radians per half cycle. When there is no conducting overlap between the two thyristors on same arm, the magnitude of the output line current clearly varies linearly with the dc link current.

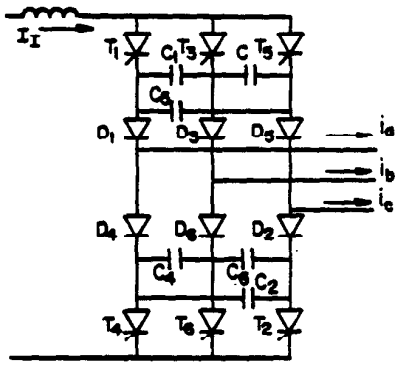

Fig. 2 Power Circuit of Auto-Sequentially Commutated Current Source Inverter.

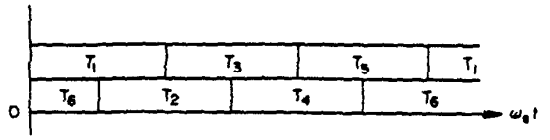

Fig. 3 Firing Time Sequence for Each Thyristor for Normal ASCI.

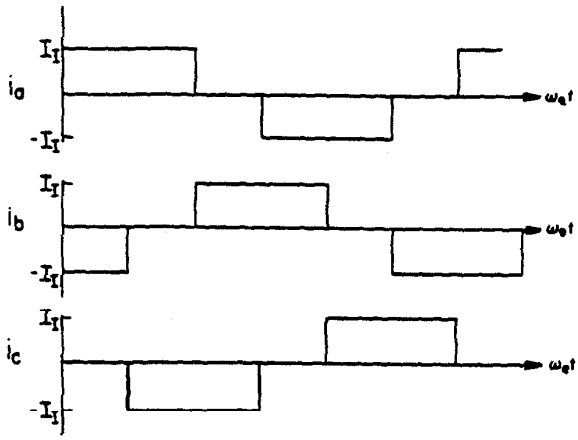

Fig. 4 Ideal Motor Line Current Supplied from ASCI.

Consider now the firing method for the NASCI. In this case the dc link current remains fixed. The thyristors are fired in such a manner to make an intentional conducting overlap between the two thyristors on same arm in the inverter. The two thyristors, in effect, short the dc source and form a current bypass in parallel with the load. By varying the shorting time, the output ac current to the load can clearly be varied. In order to realize this firing scheme, additional firing signals must be introduced at certain instants of the firing time sequence as shown in Fig. 5 where the numbers correspond to the numbered thyristors in Fig. 2. Fig. 6 shows the resulting ac line current with a passive three phase load. It can be noted that there is a notch at the middle position of the current wave compared to the wave in Fig. 4.

Fig. 7 details of notched current wave. It can be observed that from the symmetrical arrangement of the short circuit time of two thyristors on same arm in the inverter, the current wave consists of two identical square pulses during each half cycle. The width of each pulse is described by a quantity θ and the width of the notch between the two pulses is described by a quantity W. From Fig. 7 it is known that the angle θ is equal to $\pi/3 - W$ and it is obvious that the ac current wave can be expressed as a symmetric even function, i.e, $i(\omega_e t) = i(-\omega_e t)$. The Fourier Series expansion of the current wave of Fig. 7 can be represented by

$$i_a = \frac{4\sqrt{3}}{\pi} I_l \left[\sin\frac{\theta}{2}\cos\omega_e t - \frac{1}{5}\sin\frac{5\theta}{2}\cos 5\omega_e t + \frac{1}{7}\sin\frac{7\theta}{2}\cos 7\omega_e t - \frac{1}{11}\sin\frac{11\theta}{2}\cos 11\omega_e t + \cdots \right] \quad (1)$$

Similar equations apply for the b and c phase currents which are appropriately phase shifted forward or backward in time by 120 electrical degrees.

To simplify the analysis and simulation study the following assumptions have been adopted. 1) The dc link current I_l is constant. 2) The effect of harmonics are neglected. 3) Commutation between two phases of motor is assumed to be ideal with zero commutation overlap. Under such conditions, Eq. 1 can be expressed by

$$i_a = \frac{4\sqrt{3}}{\pi} I_l \sin\frac{\theta}{2}\cos\omega_e t \quad (2)$$

One can observe from Eqs. 1 and 2 that in addition to the current control usually obtained by manipulating the dc link current I_l, the ac current can also clearly be adjusted by means of the angle θ. Specifically, the fundamental current varies as the sine of the angle θ. Linearity between the current command and the fundamental component of output current can be retained by compensation with an inverse sine function. Although notch control of the output current waveform is a relatively straightforward modification to the ASCI thyristor control it can be shown that the dynamic and transient behavior of such a system is substantially improved. To demonstrate the degree of improvement that can be obtained two typical classes of control systems of ac induction machine drives are considered. The first system is typically utilized for general industrial drives while the other finds application in fast response servo drives.

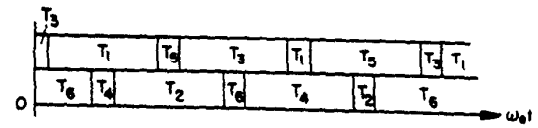

Fig. 5 Firing Time Sequence for Each Thyristor in NASCI.

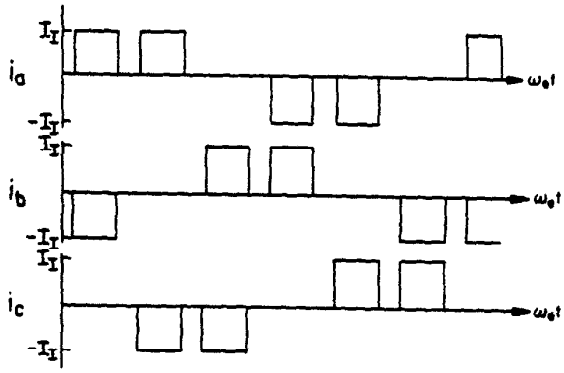

Fig. 6 Ideal Motor Line Current Supplied from NASCI.

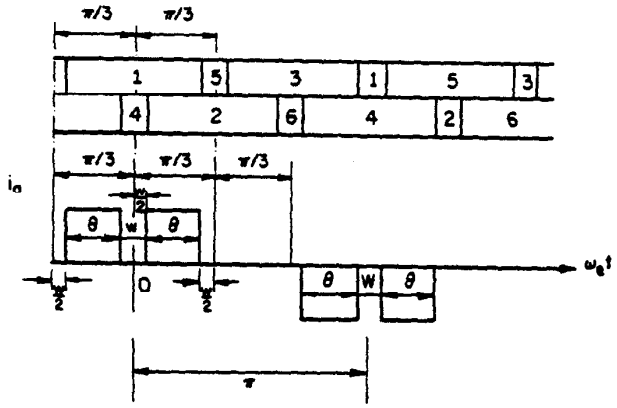

Fig. 7 Detailed Illustration of Load Line Current Waveform of NASCI.

TORQUE CONTROL WITH SLIP FREQUENCY AND CURRENT REGULATION

In this section the general purpose drive will be considered. The system of concern consists of a rectifier, a dc link reactor, a NASCI and an induction machine (or simply a NASCI-IM system). Although the mode of operation of the NASCI is different from the operating mode of an ASCI, in substance, both types are current sources. Hence, the steady state operating characteristics of a current source inverter driven induction machine remains valid for a NASCI-IM drive. From the per phase equivalent circuit of the induction machine, Fig. 8, it can be noted that if the input variable is considered as the stator current I_s, then the following two equations can be obtained

$$I_r' = \frac{\left|jX_m I_s\right|}{\left|R_r'/S + jX_r'\right|} \tag{3}$$

$$T_e = \frac{3P}{2\omega_e}\frac{I_r'^2 R_r'}{S} \tag{4}$$

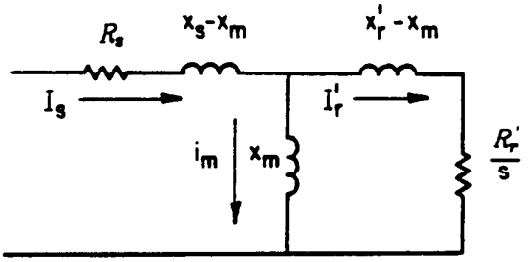

Fig. 8 Conventional Equivalent Circuit of Induction Machine.

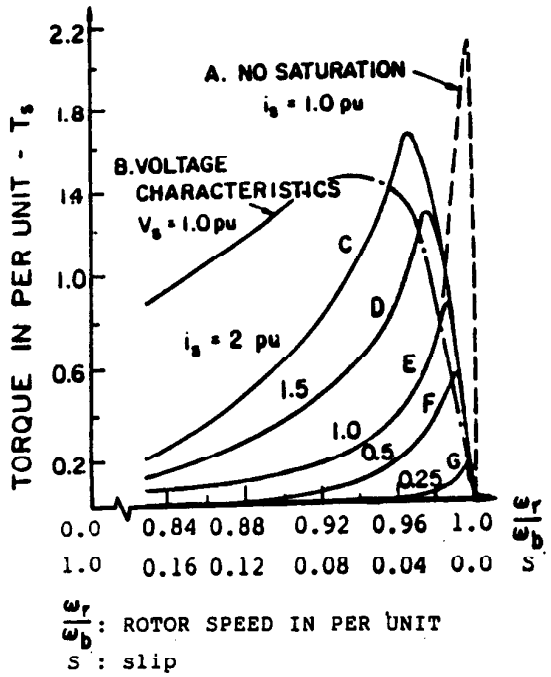

Fig. 9 Torque-Speed Curves for Controlled Current Operation of Induction Machine.

The steady state torque-speed characteristics of the motor with current source excitation can readily be calculated from the above two equations. The resulting torque-speed curve is shown in Fig. 9, curve A. The 18.6 kw motor parameters used for this curve are given in Appendix I. It can be noted that this curve is essentially the same as the detailed solution contained in Ref. 3 even though harmonics have been neglected in this analysis.

The slip frequency/current control scheme adopted by the authors is shown in Fig. 10. In order to explain the control principle, the torque-speed curve of the motor under constant voltage source operation can be constructed as in Fig. 9, curve B. The control principle in Fig. 10 is employed to utilize the quasi-linear operating range of torque-speed curve B. Hence, the motor is controlled to provide good torque per ampere near its rated flux. According to this principle the motor operates at a series of working points which are the intersection of points on the voltage source torque-speed curve B and a group of current source torque-speed curves of the motor, curves C to G.

In Fig. 10 a proportional and integral (PI) regulator is used to control the motor speed. The output of the speed regulator is used to develop a slip frequency command. The slip frequency and rotor speed are sent to a summer to form the stator frequency set point. The slip frequency is multiplied by a factor and is also used to control the set point of the angle θ. A magnitude limiter at the output terminal of the speed regulator controls the maximum slip frequency, i.e controls the maximum output torque of the motor. The control scheme in Fig. 10 is very similar to the conventional control discussed in Ref. 4. However, it can be noted that in this case the dc link current is independently controlled to keep its value constant at the desired value. Also, the amplitude of the fundamental component of ac output current of the inverter is controlled by the angle θ^* which is, in turn, proportional to the slip frequency. It can be noted that the stator frequency set point ω_e^* and angle set point θ^* are both utilized to adjust the firing instants of these thyristors in the inverter to obtain the desired current.

It is useful to now consider the dynamic behavior of the system of Fig. 10. The differential equations which describe the transient behavior of an induction machine can be conveniently expressed by a set of $d-q$ equations. When the $d-q$ reference frame rotates synchronously with the air-gap MMF, i.e with synchronous speed, these equations are expressed in the following form,

$$\begin{bmatrix} v_{qs} \\ v_{ds} \\ 0 \\ 0 \end{bmatrix} = \begin{bmatrix} R_s + pL_s & \omega_e L_s & pL_m & \omega_e L_m \\ -\omega_e L_s & R_s + pL_s & -\omega_e L_m & pL_m \\ pL_m & \omega_{sl} L_m & R_r' + pL_r' & \omega_{sl} L_r' \\ -\omega_{sl} L_m & pL_m & -\omega_{sl} L_r' & R_r' + pL_r' \end{bmatrix} \begin{bmatrix} i_{qs} \\ i_{ds} \\ i_{qr}' \\ i_{dr}' \end{bmatrix} \tag{5}$$

$$T_e = \frac{3}{2}\frac{P}{2} L_m \left(i_{qs} i_{dr}' - i_{ds} i_{qr}' \right) = T_l + \frac{2}{P} jp\omega_r \tag{6}$$

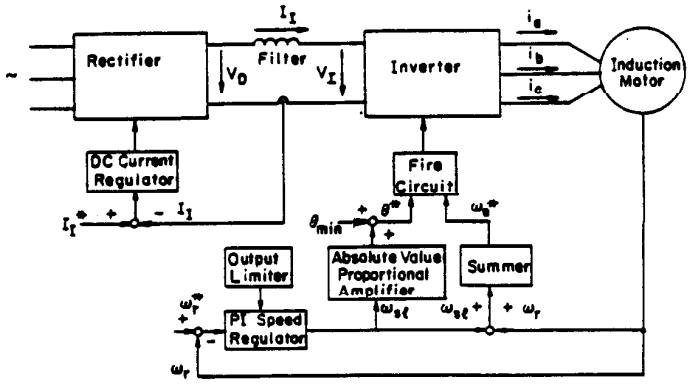

Fig. 10 Block Diagram of NASCI-IM Drive System under Slip Frequency Current Regulation

From Fig. 10 the control equations of the system can be written as

$$\omega_{sl} = \frac{k_1 (1 + \tau_1 p)}{p} (\omega_r^* - \omega_r) \quad (7)$$

$$\omega_e = \omega_{sl} + \omega_r \quad (8)$$

$$\theta = \theta_{\min} + \beta \left| \omega_{sl} \right| \quad (9)$$

Applying the synchronous reference frame transformation to the three phase set of currents implied by Eq. 2 and choosing an alignment of the $q-$axis with the a phase axis of the motor at time $t = 0$, the corresponding $q-$ and $d-$ axis currents in the synchronous frame become

$$i_{qs} = \frac{4\sqrt{3}}{\pi} I_1 \sin(\frac{\theta}{2}) \quad (10)$$

$$i_{ds} = 0 \quad (11)$$

Referring to Fig. 7, it can be noted that the range of the angle θ is $0 \le \theta \le \pi/3$. In this range $\sin\theta/2 \approx \theta/2$. Equation 10 can then be reduced to

$$i_{qs} \approx \frac{4\sqrt{3}}{\pi} I_1 \frac{\theta}{2} = \frac{2\sqrt{3}}{\pi} I_1 \theta \quad (12)$$

Upon combining Eqs. 9 and 12,

$$i_{qs} = \frac{2\sqrt{3}}{\pi} I_1 (\theta_{\min} + \beta \left| \omega_{sl} \right|) = I_{\min} \pm \alpha \omega_{sl} \quad (13)$$

In Eq. 13, when $\omega_{sl} \ge 0$ then the "+" symbol applies whereas when $\omega_{sl} < 0$ then "−" is used. In addition, it is useful to define

$$\alpha = \frac{2\sqrt{3}}{\pi} I_1 \beta \quad (14)$$

and

$$I_{\min} = \frac{2\sqrt{3}}{\pi} I_1 \theta_{\min} \quad (15)$$

where $\theta_{\min}$ is the permitted minimum value of the angle θ. The value of $\theta_{\min}$ depends on the commutation limit and is also related to desired $I_{\min}$ and I_1. The quantity $I_{\min}$ is the desired minimum current of the motor. In this paper $I_{\min}$ is selected as the rated exciting current, i.e the ideal no load stator current. The value of I_1, a constant in this control algorithm, is a function of the maximum desired output torque of the motor.

The torque and speed behavior of the motor for this system can be described by Eqs. 5-8 and 13. Note that $i_{ds} = 0$ in Eq. 11 and $i_{qs} = I_{\min} \pm \alpha\omega_{sl}$ in Eq. 13, in which $I_{\min}$ is constant. In this case it can be determined that there are only four independent state variables which describe the speed and torque dynamics of the motor. After dealing with the above equations, the dynamic properties of the motor drive can be described by matrix Eq. 16,

$$\begin{bmatrix} p & 0 & 0 & k_1 + k_1\tau_1 p \\ \pm L_m \alpha p & R_r' + L_r' p & L_r' \omega_{sl} & 0 \\ -L_m (\pm \alpha\omega_{sl} + I_{\min}) & -L_r' p \omega_{sl} & R_r' + L_r' p & 0 \\ 0 & 0 & \frac{3}{4} L_m (\pm \alpha\omega_{sl} + I_{\min}) & -\frac{2}{P} Jp \end{bmatrix} \times \begin{bmatrix} \omega_{sl} \\ i_{qr}' \\ i_{dr}' \\ \omega_r \end{bmatrix} = \begin{bmatrix} k_1 + k_1\tau_1 p \\ 0 \\ 0 \\ 0 \end{bmatrix} \omega_r^* + \begin{bmatrix} 0 \\ 0 \\ 0 \\ 1 \end{bmatrix} T_l \quad (16)$$

The following matrix can be used to calculate other important system variables

$$\begin{bmatrix} v_{qs} \\ v_{ds} \\ \omega_e \end{bmatrix} = \begin{bmatrix} \pm \alpha(R_s + L_s p) & L_m p & L_m \omega_e & 0 \\ \pm \alpha L_s (-\omega_e) & -L_m \omega_e & -L_m p & 0 \\ 1 & 0 & 0 & 1 \end{bmatrix} \begin{bmatrix} \omega_{sl} \\ i_{qr}' \\ i_{dr}' \\ \omega_r \end{bmatrix} + \begin{bmatrix} R_s + pL_s \\ -L_s \omega_e \\ 0 \end{bmatrix} I_{\min} \quad (17)$$

Again the "+" ("-") sign is used when the slip is positive (negative).

The dynamic properties of the system can now be established by linearization of Eq. 16 [5]. The resulting small signal equation relating the state variables to the speed command and load torque inputs is

$$\begin{bmatrix} p & 0 & 0 \\ \pm L_m \alpha p + L_r' i_{qr0} & R_r' + L_r' p & L_r' \omega_{sl0} \\ \pm 2L_m \alpha(-\omega_{sl0}) - L_m I_{\min} - L_r' i_{qr0} & -L_r' \omega_{sl0} & R_r' + L_r' p \\ \pm \frac{3P}{4} L_m \alpha i_{dr0} & 0 & \pm \frac{3P}{4} L_m \alpha \omega_{sl0} + \frac{3P}{4} L_m I_{\min} \end{bmatrix} \begin{bmatrix} k_1 + k_1\tau_1 p \\ 0 \\ 0 \\ \frac{-2}{P} J p \end{bmatrix} \times \begin{bmatrix} \Delta\omega_{sl} \\ \Delta i_{qr}' \\ \Delta i_{dr}' \\ \Delta\omega_r \end{bmatrix} = \begin{bmatrix} k_1 + k_1\tau_1 p \\ 0 \\ 0 \\ 0 \end{bmatrix} \Delta\omega_r^* + \begin{bmatrix} 0 \\ 0 \\ 0 \\ 1 \end{bmatrix} \Delta T_l \quad (18)$$

The matrix Eq. 18 can be explicitly expressed as

$$\begin{bmatrix} 1 & 0 & 0 & k_1\tau_1 \\ \pm L_m \alpha & L_r' & 0 & 0 \\ 0 & 0 & L_r' & 0 \\ 0 & 0 & 0 & -\frac{2}{P} J \end{bmatrix} p \begin{bmatrix} \Delta\omega_{sl} \\ \Delta i_{qr}' \\ \Delta i_{dr}' \\ \Delta\omega_r \end{bmatrix} =$$

$$\begin{bmatrix} 0 & 0 & 0 \\ -L_r' i_{qr0} & -R_r' & -L_r' \omega_{sl0} \\ \pm 2L_m \alpha\omega_{sl0} + L_m I_{mn} + L_r' i_{qr0} & L_r' \omega_{sl0} & -R_r' \\ \pm \frac{3P}{4} L_m(-\alpha) i_{dr0} & 0 & \pm \frac{3P}{4} L_m(-\alpha)\omega_{sl0} - \frac{3P}{4} L_m I_{mn} \end{bmatrix} \begin{bmatrix} -k_1 \\ 0 \\ 0 \\ 0 \end{bmatrix} \times \begin{bmatrix} \Delta\omega_{sl} \\ \Delta i_{qr}' \\ \Delta i_{dr}' \\ \Delta\omega_r \end{bmatrix} + \begin{bmatrix} k_1 \\ 0 \\ 0 \\ 0 \end{bmatrix} \Delta\omega_r^* + \begin{bmatrix} k_1 \\ 0 \\ 0 \\ 0 \end{bmatrix} p\Delta\omega_{rg} + \begin{bmatrix} 0 \\ 0 \\ 0 \\ 1 \end{bmatrix} \Delta T_l \quad (19)$$

The output equation required to obtain speed from the state variables is

$$\Delta\omega_r = \begin{bmatrix} 0 & 0 & 0 & 1 \end{bmatrix} \begin{bmatrix} \Delta\omega_{sl} & \Delta i_{qr}' & \Delta i_{dr}' & \Delta\omega_r \end{bmatrix}^T \quad (20)$$

where T denotes the transpose.

A digital computer algorithm can be used to evaluate Eqs. 19 and 20 to find the transfer function between the output $\Delta\omega_r$ and the input $\Delta\omega_r^*$ [5]. The results of such calculations at typical operating points are shown in Tables 1 and 2. The results of the two tables correspond to two different sets of parameters of the speed regulator. From these results it can be seen that the motor drive is capable of operating in a stable manner over a fairly wide range of the control gain k_1 and also has very good damping properties except for the case of very light load conditions. The problem of light damping at no load has been documented previously in the literature [2,6].

It is useful to compare the results in Table 2 with the results in Table 9 of Ref. 6, which lists the poles and zeros for ASCI-IM drive system with a similar slip frequency current regulation. It is not difficult to determine three distinguishing characteristics for the NASCI-IM system:

1) The poles and zeros in the NASCI system are not related to the rotor speed. In fact this also can be seen from the matrix Eq. 16, since it can be determined that there are no stator frequency terms ω_e in the matrix. Hence, the dynamics of the system are not related to stator frequency. Note that in Eq. 8 $\omega_e = \omega_r + \omega_{sl}$. Therefore, for certain slip frequency operating points the system dynamic property is independent of the rotor speed whereas the poles and zeros in the corresponding ASCI-IM system is related to rotor operation speed [6].

2) For certain values of motoring torque and braking torque, i.e certain absolute slip frequency values, the poles and zeros are identical in the NASCI-IM system. However, they are different for identical values of motoring torque and braking torque in the ASCI-IM system, (see Table 9 in [6]).

3) For the NASCI-IM system increasing the control gain k_1 of the system tends to speed up the response of the system. This feature can be observed by checking the values in Table 1 and Table 2. This trend is a desirable feature for the design of an ac adjustable speed system since the control gains are set with relative simplicity.

The conclusions reached by the small signal analysis has been verified by a detailed analog computer simulation. The analog computer simulation traces in Fig. 11 show the waveform of the motor phase current and phase voltage supplied from a NASCI. The traces in Fig. 12 show the torque response of the motor when the same motoring or braking load is applied at two different speeds. One can note that nearly the same transient behavior is obtained for the two cases. Fig. 13 shows the simulation traces of torque and speed response of the motor corresponding to two sets of parameters of the speed regulator given in Table 1 and Table 2. Note that one gain is 0.25, another is 10, and response is clearly faster for the case of greater gain.

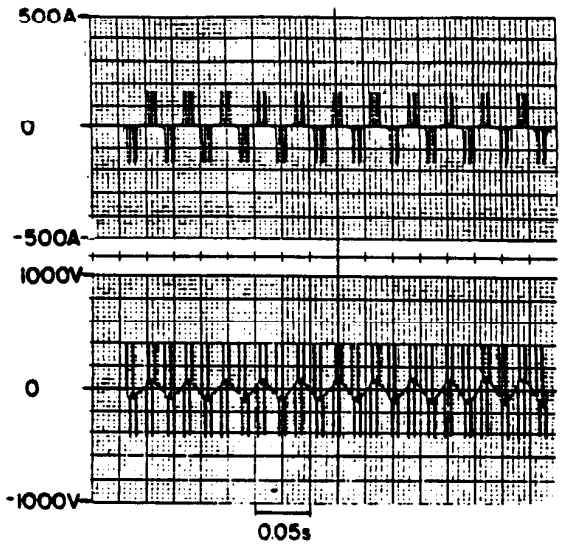

Fig. 11 AC Phase Current and AC Phase Voltage of Induction Machine Supplied from NASCI.

Table 1 Transfer Function $\Delta\omega_r / \Delta\omega_r^*$ $k_1 = 0.25$ $\tau_1 = 1.0$

T_e (nm)	f_w (hz)	DC gain	Zeros	Poles
0.0	0.0	1.0	-2.563	-0.7648 ± j 6.847 -2.563 -1.033
± 2.26	± 0.02	1.0	-2.635 -86.76	-1.040 ± j7.141 -2.633 -1.030
± 29.6	± 0.2	1.0	-2.861 -13.0	-3.848 ± j8.278 -3.618 -1.030
± 102.5	± 1.05	1.0	-4.623 ± j4.406	-5.625 ± j8.489 -3.618 -1.188
± 153.9	±2.2	1.0	-4.215 ± j11.81	-4.031 ± j14.55 -5.672 -1.188

Table 2 Transfer function $\Delta\omega_r / \Delta\omega_r^*$ $k_1 = 10.0$ $\tau_1 = 0.5$

T_e (nm)	f_w (hz)	DC Gain	Zeros	Poles
0.0	0.0	1.0	-2.563	-0.2803 ± j31.3 -2.563 -2.002
±2.26	±0.02	1.0	-2.635 -86.78	-6.419 ± j32.09 -2.634 -2.002
±29.6	±0.2	1.0	-2.861 -13.00	-14.66 ; -112.7 -2.849 ; -2.006
±102.5	±1.05	1.0	-4.623 ±j4.406	-4.752 ±j4.333 -212.2 -2.032
±153.9	±2.2	1.0	-4.215 ± j11.81	-4.412 ± j11.84 -199.6 -2.028

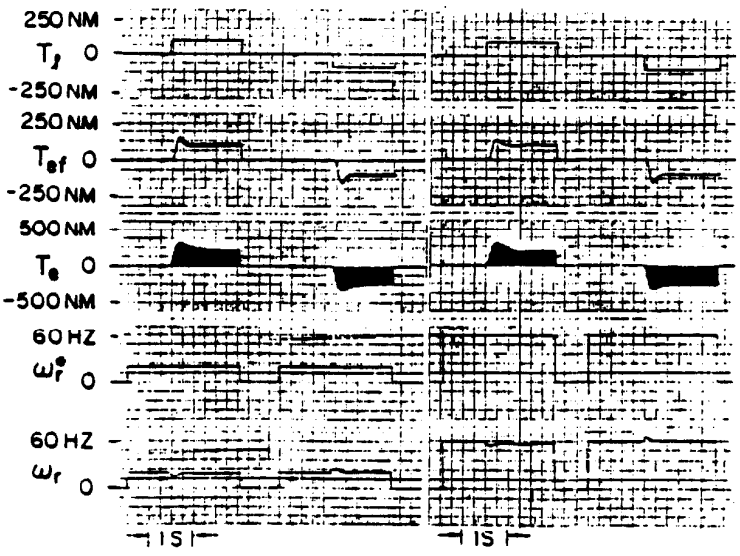

Fig. 12 Simulation Traces of Torque and Speed Response of NASCI-IM Drive with Same Amplitude Motoring or Braking Torque at Different Operation Speeds Using Control Scheme of Fig. 10 ($K_1 = 0.25$ $\tau_1 = 1.0$)

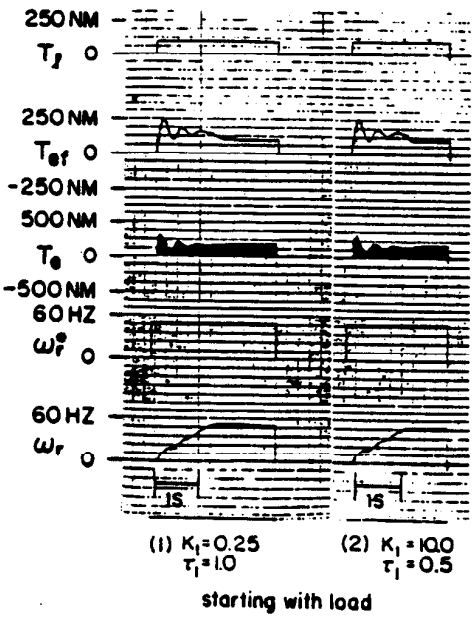

Fig. 13 Simulation Traces of Torque and Speed Response of NASCI-IM System with Different Control Gain Using Control Scheme of Fig. 10

FIELD ORIENTED CONTROL OF NASCI-IM DRIVE SYSTEM

When there is a demand for high quality, fast response performance the field orientation method of ac induction machine control often is utilized. In this case the performance equations of an induction machine can be described by the following set of equations in the $d-q$ reference axes rotating at synchronous speed ω_e,

$$v_{qs} = R_s i_{qs} + p\lambda_{qs} + \omega_e \lambda_{ds} \quad (21)$$

$$v_{ds} = R_s i_{ds} + p\lambda_{ds} - \omega_e \lambda_{qs} \quad (22)$$

$$0 = R_r' i_{qr}' + p\lambda_{qr}' + \omega_{sl}\lambda_{dr}' \quad (23)$$

$$0 = R_r' i_{dr}' + p\lambda_{dr}' - \omega_{sl}\lambda_{qr}' \quad (24)$$

$$\lambda_{qs} = L_s i_{qs} + L_m i_{qr}' \quad (25)$$

$$\lambda_{ds} = L_s i_{ds} + L_m i_{dr}' \quad (26)$$

$$\lambda_{qr}' = L_m i_{qs} + L_r' i_{qr}' \quad (27)$$

$$\lambda_{dr}' = L_m i_{ds} + L_r' i_{dr}' \quad (28)$$

$$T_e = \frac{3}{2}\frac{P}{2}\frac{L_m}{L_r'}\left(\lambda_{dr}' i_{qs} - \lambda_{qr}' i_{ds}\right) \quad (29)$$

If the instantaneous speed of the rotor flux vector is chosen to be the synchronous speed in the above equations, and the phase between the reference frame axes and the two components of the rotor flux is locked in such a way that the rotor flux is entirely in the d-axis, then

$$\lambda_{qr}' = 0 \quad (30)$$

$$\lambda_{dr}' = \lambda_r' \quad (31)$$

The positions of the $d-q$ stator currents and rotor flux are shown in Fig. 14 with this choice of reference. If the rotor flux is controlled only by the stator current component i_{ds} then field orientation is said to be realized in the induction machine.

Since field orientation implies that $\lambda_{qr}' = 0$ the torque expression, Eq. 29, reduces to

$$T_e = \frac{3}{2}\frac{P}{2}\frac{L_m}{L_r'}\lambda_{dr}' i_{qs} \quad (32)$$

It is apparent that the torque only depends on two variables, λ_{dr}' and i_{qs}.

Combining Eqs. 24,28 and 30 the following expression can be obtained

$$\lambda_{dr}' = \frac{R_r' L_m}{R_r' + L_r' p} i_{ds} = \frac{L_m}{1 + T_r p} i_{ds} \quad (33)$$

In Eq. 33 the quantity T_r is the open circuit rotor time constant. It is apparent from Eq. 33 that the rotor flux can only exponentially change with a change in input current. Hence, it is not easy to realize fast torque control by adjusting the rotor flux λ_{dr}'. However, if the flux λ_{dr}' is kept constant, the torque of motor can almost instantaneously follow the change of current i_{qs}. In this case, fast changes of motor torque totally depends on how rapidly the current i_{qs} can be changed. The NASCI-IM drive system is very suitable for this purpose since its inverter can change its output current very rapidly by simply changing the angle θ.

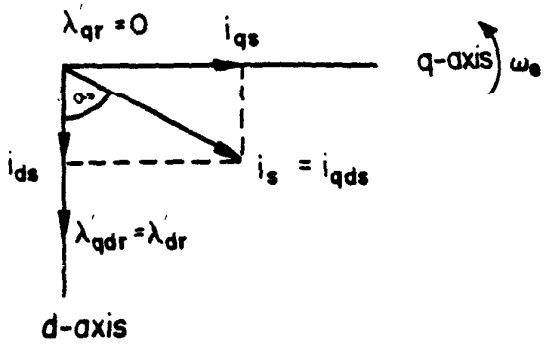

Fig. 14 Positions of d-q Stator Current with Reference Axes Oriented with the Rotor Flux.

A type of direct field orientation control adopted by authors in their simulation study is shown in Fig. 15. The position of the rotor flux vector on the stator reference frame can be sensed by using a rotor field orientor (block "RFO" in Fig. 15). The function of the rotor field orientor "RFO" is to realize following calculations

$$v_{qs} = \frac{2}{3} v_{as} - \frac{1}{3} v_{bs} - \frac{1}{3} v_{cs} \quad (34)$$

$$v_{ds} = \frac{1}{\sqrt{3}}\left(v_{cs} - v_{bs}\right) \quad (35)$$

$$i_{qs} = \frac{2}{3} i_{as} - \frac{1}{3} i_{bs} - \frac{1}{3} i_{cs} \quad (36)$$

$$i_{ds} = \frac{1}{\sqrt{3}}\left(i_{cs} - i_{bs}\right) \quad (37)$$

$$\lambda_{qs} = \int \left(v_{qs} - R_s i_{qs}\right) dt \quad (38)$$

$$\lambda_{ds} = \int \left(v_{ds} - R_s i_{ds}\right) dt \quad (39)$$

$$\lambda_{qr}' = \frac{L_r'}{L_m}\left(\lambda_{qs} - L_l i_{qs}\right) \quad (40)$$

$$\lambda_{dr}' = \frac{L_r'}{L_m}\left(\lambda_{ds} - L_l i_{ds}\right) \quad (41)$$

$$L_l = \left(L_s L_r' - L_m^2\right)/ L_r' \quad (42)$$

$$\lambda_r' = \sqrt{\lambda_{qr}'^2 + \lambda_{dr}'^2} \quad (43)$$

$$\theta_{rf} = \tan^{-1}\frac{\lambda_{qr}'}{\lambda_{dr}'} \quad (44)$$

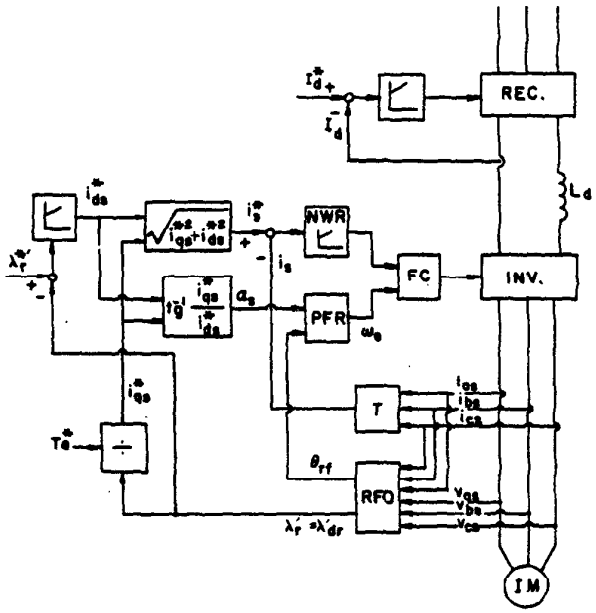

Fig. 15 Block Diagram of Direct Field Orientation Control of NASCI-IM Drive.

In these equations λ_r' is the amplitude of the rotor flux, while the angle θ_{rf} is the rotating angle of the rotor flux in the stator reference frame.

From Fig. 14 it can be seen that if field orientation is maintained, the angle α_s between the rotor flux λ_r' and the stator current i_s should be

$$\alpha_s = \tan^{-1} \frac{i_{qs}^*}{i_{ds}^*} \tag{45}$$

The position of the stator current in the stator reference frame can now be obtained from the values of θ_{rf} and the angle α_s. These operations are performed by a phase and frequency regulator of stator current (block "PFR" in Fig. 15). The amplitude of the stator current is obtained from the following equation

$$i_s^* = \sqrt{i_{qs}^{*2} + i_{ds}^{*2}} \tag{46}$$

A high gain PI regulator (block "NWR" in Fig. 15) is used to control the width of angle θ to maintain very rapid stator current response to the command signal i_s^*.

A simulation study of above scheme has been completed. In the simulation the command value of rotor flux $\lambda_r'^*$ is maintained constant. The simulation results indicating torque response are shown in Fig. 16. It can be observed that the torque response is nearly instantaneous. (The order of the resulting torque response time at rated speed is about 1-2 milliseconds).

For the purpose of comparison another group of simulation traces are shown in Fig. 17. These curves are obtained for a conventional ASCI-IM drive system under a direct field orientation control scheme similar to that in Fig. 15 (The block diagram of the system is not shown in this paper). The machine parameters for simulation cases of both NASCI-IM and ASCI-IM drives are kept the same. Comparison of Figs. 16 and 17 clearly demonstrates that the torque response of ASCI-IM system is slower particularly when the speed becomes higher.

It should be pointed out that the torque response time of a NASCI-IM type of fast response servo drive would be influenced only by a random small control delay time, which mainly depends on the modulation manner of the notching. At low operation frequency, the control delay time will become longer because the control sample interval tends to become longer. However, this control delay can be reduced by increasing the number of notches in the current wave. Such a change in notch number would not be difficult to realize at low frequency. Schemes for improving the harmonic content of the NASCI output current which are suggested in next section also have the function of reducing the control delay. From the point of view of the theoretical analysis, the control delay time of NASCI can be reduced to 1 millisecond or less.

In comparison to the NASCI-IM system the torque response of the ASCI-IM drive is influenced by rectifier phase control delay time, the rated value of the rectifier output voltage, the gain of the dc current loop, and the parameters of the dc link inductor. The average phase control delay time of a three phase rectifier bridge is about 1.4 millisecond when the source frequency is 60 Hz and cannot be further reduced. The mechanism of other factors that influence the current response can be explained by using the expression

$$I_l = \frac{V_{DR} - V_l}{R_d} \frac{1}{1 + T_d p} \tag{47}$$

In this equation V_{DR} is the rated output voltage of the rectifier, I_l is dc link current, V_l is the voltage across inverter and T_d is the time constant of dc link reactor. It is useful to let

$$I_{DM} = \frac{V_{DR} - V_l}{R_d} \tag{48}$$

The quantity I_{DM} is a hypothetical dc steady current if a dc voltage $V_{DR} - V_l$ were supplied to the DC link inductor. Upon combining Eqs. 47, 48,

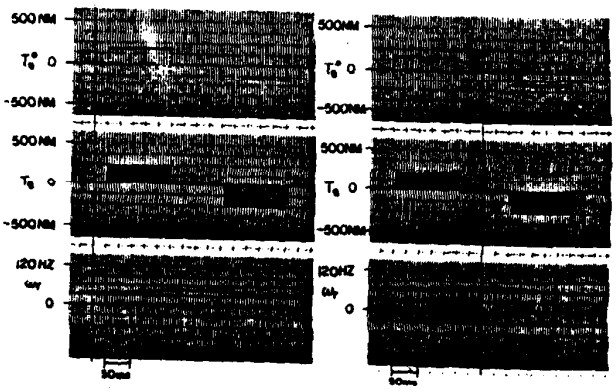

Fig. 16 Illustration of Torque Response Time of NASCI-IM Drive System with Field Orientation Control.

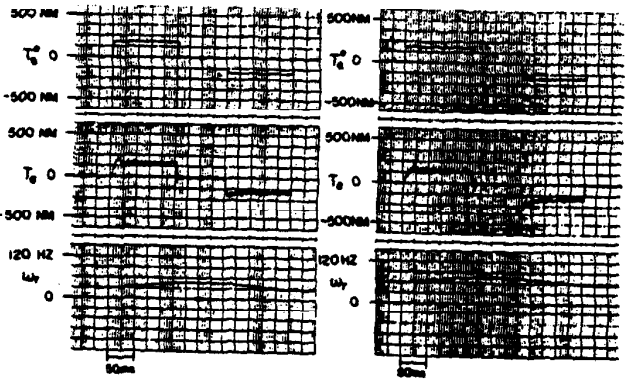

Fig. 17 Illustration of Torque Response Time of ASCI-IM Drive System with Field Orientation Control.

$$I_l = I_{DM} \frac{1}{1 + T_d p} \tag{49}$$

From Eq. 49 it is clear that the greater the value of I_{DM}; the shorter time needed to reach a certain value of I_l.

Eqs. 48 and 49 show that increasing the rated value of the rectifier output voltage V_{DR} makes the current I_{DM} greater, and hence, the current response becomes faster. However, raising the rated voltage of the rectifier will increase the equipment cost. (In the simulation study of this paper the rated voltage of the rectifier is assumed to be 1.15 times the value needed to produce the rated stator voltage of the motor). The influence of rotor speed to current response also can be seen from the Eqs. 48 and 49. As the rotor speed increases the inverter voltage V_l increases so that current I_{DM} becomes less and the current response becomes slower. The worst case occurs at rated rotor speed. The dominant factor that influences the current response is the inductance L_d of the dc link inductor. The following approximate equation can be used to estimate the DC link current response time under the influence of L_d

$$\Delta T \approx \frac{L_d \Delta I_l}{V_{DR} - V_l} \tag{50}$$

In the simulation study of this paper the inductance of the dc link reactor is about 4.5 times the short circuit inductance of the induction machine. The calculation for the simulation data shows that the dc current changes from a small value corresponding to zero torque to a maximum value corresponding to maximum torque takes about 18 milliseconds at rated speed and about 4.5 milliseconds at half speed. While the simulation traces in Fig. 17 show that the torque changes from zero value to maximum value takes about 25 milliseconds at rated speed and about 15 milliseconds at

half speed (under motoring operation). The reason that the calculation values of dc current response time are smaller than their corresponding values of torque response time from the analog computer simulation traces is because in the calculation an instantaneous DC voltage response is assumed, which means that the current control loop delay time is neglected and the dc voltage steps instantaneously to its rated value. Obviously, decreasing the inductance of the dc link inductor can speed up the current response. However, too small a value of inductance will increase the current ripple and will limit the value of the current loop gain to avoid unstable oscillations under light load conditions (ripple instability). Hence, it is very difficult to design an ASCI-IM system in which the current response time is shorter than 5 milliseconds within its entire speed range.

EFFECT OF HARMONICS AND HARMONIC MINIMIZATION

Although the torque response of the NASCI-IM drive system is improved substantially compared to a standard ASCI, the effect of the notching on the harmonic content becomes a difficult problem of concern. From Eq. 1 it can be observed that the amplitude of each current harmonic is related to the control angle θ. Table 3 shows the per unit magnitude of each current harmonic at several typical angles wherein the amplitude of fundamental component at selected values of θ is chosen as the base value. Note that when $\theta = 60°$ the current wave of NASCI is identical to that of the ASCI, so that the harmonics of the NASCI at 60° are identical to those of an ASCI. Table 3 also shows the per unit value of the total *rms* current at various angles θ. It can be noted that for the same fundamental component, the power loss increases with decreasing values of θ.

In practice, the angle θ must remain within the limits $0° < \theta < 60°$. Also, the demand for an adjustable output ac current imposes certain limits on the range of θ. Considering both aspects, the range of the angle θ is herein restricted to the range $10° < \theta < 50°$. Further, due to requirements for an overload capability, the angle θ corresponding to rated output torque has been set to 30 °. Under such conditions the heating effect for different fundamental current components, i.e at different values of θ, is shown in Table 4. In this table the dc link current I_I remains unchanged for each angle θ.

It is useful to compare the *rms* current requirements for the NASCI inverter to those for the more conventional ASCI scheme. In the case of a NASCI – IM drive, $\theta = 30°$ is chosen to correspond to rated output torque. Upon checking Table 3 it can be noted that the per unit total *rms* current at this angle value is 1.416. Clearly, if the heating limits are kept unchanged the rated output power (or torque) of the motor must be reduced. The reduction ratio is 1/ 1.416 = 0.70 compared with the case of sine wave source supplying the motor. If compared with the case of an ASCI supply then this reduction ratio will be 1.044/ 1.416 = 0.75.

A method of improving the harmonic problem in the NASCI IM drive is shown in Fig. 18. In this figure there are several schemes shown, but the basic principle is the same. That is, two groups of three phase output currents are used to supply a single machine. However, a 30° phase difference is maintained between the two groups of currents. The synthesized current wave into motor from the new scheme will be improved to the form shown in Fig. 19.

Using a Fourier series expansion of the synthesized current in Fig. 19, the per unit amplitude of each harmonic at different angles θ can be tabulated as shown in Table 5. The fundamental current at selected angles θ is still assumed to be unity. When the dc current remains unchanged, the per unit *rms* currents at various angles are shown in Table 6. In this case the fundamental current for an angle $\theta = 30°$ corresponds to the base value. Clearly, when a six phase source is adopted, the heating problem from the harmonics becomes greatly diminished. The reduction is particularly true at the angle $\theta = 30°$, which is the point that has been selected to correspond to the rated current of motor. At this point the per unit *rms* value of the current including all of the harmonics has been reduced to 1.044, referred to Table 5. Checking Table 4 and Table 6 it is found that the larger the fundamental current, the greater the improvement that can be obtained. In addition to improving the heating problem, another benefit of using multiple inverters is that the amplitude of the two lowest harmonics, the fifth and seventh, are significantly decreased. This can be observed by comparing relative values in Table 3 and 5. Such a reduction is desirable for decreasing ripple torque and improving the low frequency performance of machine. Although more power electronic elements are needed in schemes a) and b) in Fig. 19, this may not be a serious disadvantage for a large power drive system, since paralleling of power electronic elements often is already needed in

Table 3 Harmonic Currents and Total *rms* Currents at Various Angles θ when Three Phase Current Output is Adopted.

	I_1	I_5	I_7	I_{11}	I_{13}	I_{17}	I_{19}	I_{23}	I_{25}	$\sqrt{\sum I_i^2}$
10°	1.000	0.9690	0.9402	0.8544	0.7999	0.6724	0.6016	0.4521	0.3759	2.376
20°	1.000	0.8823	0.7731	0.4920	0.3393	0.0588	0.0526	0.1918	0.2165	1.712
30°	1.000	0.7464	0.5332	0.0909	0.0769	0.2196	0.1964	0.0435	0.0400	1.416
40°	1.000	0.5759	0.2886	0.1709	0.2215	0.0586	0.0526	0.1252	0.0752	1.240
50°	1.000	0.3877	0.0296	0.2143	0.1044	0.1261	0.1129	0.0590	0.0943	1.124
60°	1.000	0.2000	0.1429	0.0909	0.0769	0.0588	0.0526	0.0435	0.0400	1.044

Table 4 Fundamental Currents, Total *rms* Currents and Their Ratio at Several Angles θ (Case for 3 Phase Current Output).

Angle θ	10°	20°	30°	40°	50°	60°
I_1 (fund. current)	0.3367	0.6709	1.000	1.3215	1.6329	1.9319
I_Σ (total rms)	0.7998	1.1482	1.416	1.6379	1.8352	2.0176
I_Σ / I_1	2.376	1.712	1.416	1.240	1.124	1.044

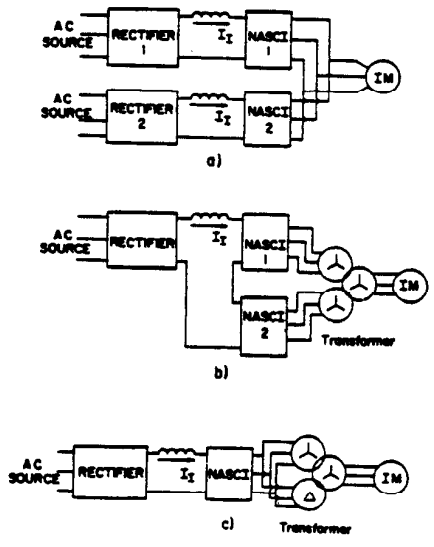

Fig. 18 Schemes of Improving Harmonics in NASCI-IM Drive.

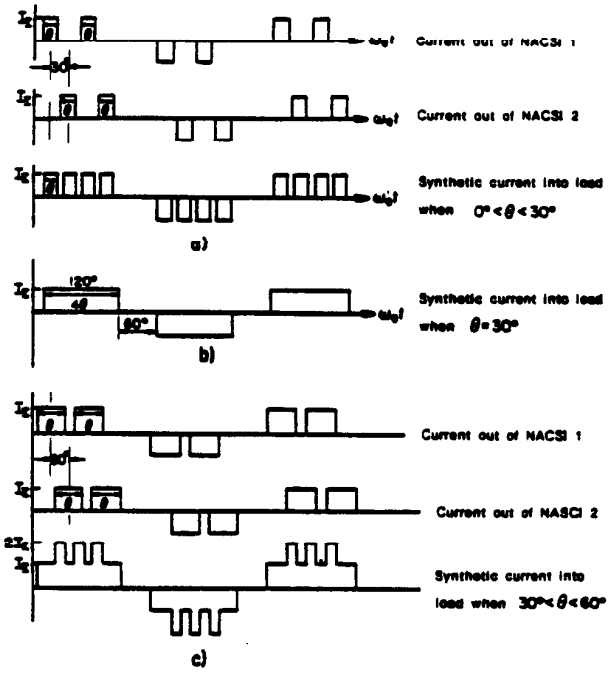

Fig. 19 Synthesized Current Wave Corresponding to the Schemes of Fig. 18.

CONCLUSION

In this paper a simple type of current wave notching has been presented. The notch operation mode of ASCI, or the NASCI operating mode is of considerable interest. In effect it is the dual mode of a voltage type PWM inverter. Theoretical and digital analysis as well as analog computer results for a NASCI- IM drive system using conventional slip-current control method were presented. Simulation traces for a NASCI-IM drive system and an ASCI-IM drive system utilizing same field orientation control also were shown. It was demonstrated that improved dynamic properties can be obtained from the NASCI drive system for both cases.

The NASCI current source has a number of novel aspects that are of importance. First, because the width but not the amplitude of the output current wave from inverter is varied, the output current into an ac load can respond to the current command very quickly. Although there is a small sample delay of current control, digital computer analysis shows that it nearly has no influence on the system except at very low operating frequency. (The analysis results are not presented in this paper). Improvement in operating performance at low frequency can be realized by simply doubling the number of the notches in the current wave for each halving of the line frequency as frequency is reduced. The methods of improving harmonics suggested in Figs. 19 a) and b) also provides such benefit.

Second, the dc link parameters and stator parameters of motor have essentially no influence on the dynamics of the motor in the NASCI drive system. This is an important feature for control system design.

Finally, the NASCI operating mode suggested here and the normal ASCI operating mode can be complementary. Hence, new control schemes may be possible which allow the inverter to operate under two modes. Using the working modes of both the ASCI and the NASCI to drive an induction machine, an overall improvement in dynamic response of the machine may be possible in many applications.

Table 5 Harmonic Currents and Total *rms* Currents at Various Angles θ when Six Phase Current Output is Adopted.

	I_1	I_5	I_7	I_{11}	I_{13}	I_{17}	I_{19}	I_{23}	I_{25}	$\sqrt{\sum I_i^2}$
10°	1.000	0.2589	0.2519	0.8544	0.7999	0.1802	0.1612	0.4521	0.3760	1.734
20°	1.000	0.2364	0.2071	0.4920	0.3393	0.0158	0.0141	0.1918	0.2166	1.253
30°	1.000	0.2000	0.1429	0.0909	0.0769	0.0588	0.0526	0.0435	0.0400	1.044
40°	1.000	0.1643	0.0719	0.1709	0.2215	0.0158	0.0141	0.1252	0.0752	1.066
50°	1.000	0.1039	0.0079	0.2143	0.1044	0.0338	0.0302	0.0590	0.0843	1.043
60°	1.000	0.0636	0.0383	0.0909	0.0769	0.0158	0.0141	0.0435	0.0400	1.013

Table 6 Fundamental Currents, Total *rms* Currents and Their Ratio at Several Angles θ (Case for 6 Phase Current Output).

Angle θ	10°	20°	30°	40°	50°	60°
I_1 (fund. current)	0.3667	0.6709	1.000	1.3215	1.6429	1.9319
I_Σ (total rms)	0.5839	0.8404	1.044	1.409	1.703	1.956
I_Σ / I_1	1.734	1.253	1.044	1.066	1.043	1.013

such cases due to limitations on the rating of individual thyristor devices.

It should also be mentioned that the NASCI mode of operation could be combined with the standard ASCI firing mode in certain applications. For example, if an inverter drive is used for a transfer line application, the overall general torque versus time duty is known within certain limits. The system could be controlled, for example, to operate normally in the six step mode until a point is reached where a rapid change in torque is required. In anticipation of this heavy load, the dc link current could be increased and the NASCI mode introduced, keeping the fundamental ac current equal to the instantaneous demand. When the heavy load then appears on the motor shaft, the system would be capable of very rapid response. After the transient load interval has passed, the dc link current could again be lowered and standard ASCI operation could resume. The approach of introducing NASCI operation when sudden torque changes occur would be even simpler for the case of a sudden unload.

ACKNOWLEDGMENTS

Authors thank Prof. D. Novotny for helpful discussions concerning the control algorithm discussed in this paper. They are also grateful to Mr. D. Zinger for his help with digital computation of the small signal transfer function. Finally, the authors are indebted to the industrial sponsors of the Wisconsin Electric Machines and Power Electronics Consortium (WEMPEC) for funds and facilities provided.

APPENDIX 1

PARAMETERS OF DC INDUCTOR

L_d = 0.00808 *h* R_d = 0.0385 *ohm*

NAMEPLATE MOTOR DATA	MOTOR PARAMETERS
18.6 kw	$R_s = 0.0788\ ohm$
4 poles	$R_r = 0.0408\ ohm$
3 phase Y connected	$L_s = 0.01526\ h$
$\omega_b = 377\ rad/sec$	$L_r = 0.01592\ h$
$J = 0.442\ kg\ m^2$	$L_m = 0.01470\ h$
$V_{rated} = 230\ V.$	
$I_{rated} = 64\ A.$	

APPENDIX 2

NOMENCLATURE

MEANING OF SUBSCRIPTS

0	steady state quantity as in i_{dr0}
d or q	equivalent two phase transformed variable as in i_{qs}
b	base quantity as in ω_b
l	the variable at input side of the inverter as in V_l
s	stator quantity as in L_s
r	rotor quantity as in L_r
sl	slip quantity as in ω_{sl}

MEANING OF SUPERSCRIPTS

*	command quantity as in ω_r^*
'	rotor quantity referred to stator side as in R_r'

VARIABLES

Δ	perturbation variable as in Δi_{qs}
k_1	speed regulator gain
τ_1	speed regulator time constant
α	constant, equal to $\frac{2\sqrt{3}}{\pi} I_l \beta$
β	constant, the ratio of θ/ω_{sl}
α_s	angle between rotor flux and stator current on rotor flux reference frame
i_{as}, i_{bs}, i_{cs}	three phase stator current variables
i_{qs}, i_{ds}	two phase q,d axis motor stator and
i_{qr}', i_{dr}'	rotor current variables
v_{qs}, v_{ds}	two phase q,d axis motor stator and
v_{qr}', v_{dr}'	rotor voltage variables
V_l	DC voltage across inverter
I_l	DC current through dc link circuit
ΔI_l	increment variable of dc link current I_l
V_{DR}	rated output voltage of rectifier
T_l, T_e	load torque, motor torque
T_{ef}	the filtered quantity of torque T_e
ω_e	motor stator angular frequency
ω_b	base angular frequency
ω_r	rotor angular frequency of 2 pole machine
P	number of poles
I_{min}	smallest stator current of motor
p	operator d/dt

REFERENCES

[1] R. W. Menzies, A. M. A. Mahmoud, "Comparison of Optimal PWM Techniques with a Bang-Bang Reference Current Controller for Voltage Source Inverter Fed Induction Motor Drives", 1983 IEEE – IAS Annual Meeting, pp. 685 – 692.

[2] E. P. Cornell, T. A. Lipo, "Modeling and Design of Controlled Current Induction Motor Drive System", 1975 IEEE – IAS Annual Meeting Sept.28 – Oct.2 1975, pp. 612 – 620.

[3] T. A. Lipo, E. P. Cornell, "State Variable Steady State Analysis of a Controlled Current Induction Machine Drive", IEEE Trans. on Ind. Applic., vol IA – 11 No.6 Nov./Dec. 1975. pp. 704 – 712.

[4] R. B. Magg, "Characteristics and Application of Current Source/Slip Regulated AC Induction Motor Drives", 1971 Industry Application Annual Meeting, pp. 411 – 413.

[5] T. A. Lipo, A. B. Plunkett, "A Novel Approach to Induction Motor Transfer Functions", IEEE Trans. Power Apparatus and Systems, vol. PAS – 93, No.5, Sept./Oct. 1974, pp. 1410 – 1418.

[6] E. P. Cornell, T. A. Lipo, "Design of Controlled Current AC Drive Systems Using transfer Function Techniques", Conference Record of IFAC Symposium on Control in Power Electronics and Electrical Drives, Duesseldorf, Oct. 7 – 9, 1974, Vol. 1, pp. 133 – 147.

[7] D. W. Novotny, T. A. Lipo, "Vector Control and Field Orientation", Tutorial Report, Univ. of Wisconsin – Madison, May, 1983, 73 pp.